Speed of sound and phase transitions in neutron stars indicated by the thick neutron skin of ^{208}Pb

Manjia Chen,[1] Dawei Guan,[1] Chongji Jiang,[1] and Junchen Pei[1,2,*]

[1]*State Key Laboratory of Nuclear Physics and Technology, School of Physics, Peking University, Beijing 100871, China*

[2]*Southern Center for Nuclear-Science Theory (SCNT), Institute of Modern Physics, Chinese Academy of Sciences, Huizhou 516000, China*

(Received 16 July 2023; revised 29 October 2023; accepted 4 December 2023; published 22 December 2023)

The speed of sound is a novel probe of equation of state and phase transitions in dense cores of neutron stars. Recently nuclear experiments extracted a surprising thick neutron skin of ^{208}Pb, causing tensions to reproduce the tidal deformability in gravitational-wave observations. This work finds that exotic structures in the speed of sound with a small softening slope followed by a steep-rising peak are required to reconcile the thick neutron skin of ^{208}Pb with astronomical observations of neutron stars. Furthermore, the peak of the speed of sound is narrowly constrained around two times the nuclear saturation density with the thick neutron skin. Consequently early and strong first-order phase transitions are comparatively more favorable.

DOI: 10.1103/PhysRevC.108.065806

I. INTRODUCTION

Dense nuclear matter is of fundamental interest to study strong interactions and the phase transition from nuclear matter to quark matter. The recent advent of astronomic observation facilities such as LIGO/Virgo [1,2] and NICER [3,4] has brought unprecedented opportunities to explore the dense cores of neutron stars. However, it is unlikely to constrain the equation of state (EoS) of dense nuclear matter by astronomical observations alone. In nuclear physics, EoS around the nuclear saturation density ($n_{\rm sat} \approx 0.16$ fm^{-3}) is largely known, providing a stepping stone for extrapolations to higher densities. It is possible to constrain EoS up to 5 times $n_{\rm sat}$ with heavy-ion collision experiments but restricted to nearly symmetric nuclear matter [5,6]. The first-principle descriptions of nuclear matter from chiral effective field theory (χEFT) also suffer from large uncertainties towards higher densities [7], due to ambiguous many-body interactions. In addition, strongly interacting matter at extremely high densities $n \gtrsim 40 n_{\rm sat}$ can be reliably calculated by the perturbative quantum chromodynamics (pQCD) [8]. Therefore the study of nuclear matter at a few times $n_{\rm sat}$, i.e., the possible scenario of phase transition, by applying constraints from multiple messengers is a destined choice.

It is always intriguing to connect properties of finite nuclei and observations of neutron stars. Among existing nuclear observables to constrain EoS, it is worthy to mention the recent PREX and PREX-II experiments on measuring the neutron skin of ^{208}Pb through parity violation in electron scattering [9,10]. The extracted neutron skin thickness is $R_{\rm skin}^{208} = 0.283 \pm 0.071$ fm [10], which is abnormally large and presents a serious challenge to current nuclear theories. Advanced *ab initio* calculations of ^{208}Pb predict a neutron skin thickness about 0.14–0.20 fm [11]. The comprehensively inferred $R_{\rm skin}^{208}$ is 0.17 fm by considering constraints of astrophysical data [12]. The large $R_{\rm skin}^{208}$ leads to a large radius and large tidal deformability of neutron stars of 1.4 solar mass ($M_\odot$), causing tensions with gravitational-wave observations in the GW170817 event [13]. The experimental neutron skin of ^{48}Ca [14] is slightly less than theoretical estimations and is not an imperative issue.

The behaviors of speed of sound in neutron stars have attracted great interests recently [15,16]. The speed of sound c_s is defined as

$$c_s^2 = \frac{\partial p(\epsilon)}{\partial \epsilon},$$

where p is the pressure and ϵ is the energy density. Therefore, EoS can be determined via an integral of c_s^2 without details of nuclear interactions [15]. The speed of sound c_s in the pQCD regime is reliably calculated to be $1/\sqrt{3}$ of the speed of light [8], providing a novel constraint on EoS at extremely high densities. Around the saturation density, the speed of sound is defined by the incompressibility of nuclear matter [17]. The speed of sound between these two regimes is essentially unknown. The allowed c_s from exhaustive searches and the possibilities of hybrid neutron stars have been extensively explored [15,16]. It is largely believed that with increasing densities, c_s should first rise to surpass $1/\sqrt{3}$ and then decrease and finally approach $1/\sqrt{3}$ [16]. The speed of sound is also a direct signature of phase transitions, in which various nonsmooth structures such as bumps, spikes, step functions, plateaus, and kinks are possible [18].

The aim of this work is to reveal the impacts of the abnormal thick neutron skin of ^{208}Pb on the speed of sound and EoS of neutron stars. There were extensive studies of consequences of the thick neutron skin of ^{208}Pb [11–13,19–24], or structures of speed of sound in neutron stars [7,15,16,18,25–30] separately. This work performs the first combined study and finds that exotic structures in speed of sound are required

*peij@pku.edu.cn

to reconcile the thick neutron skin with astronomical observations of neutron stars.

II. METHODS

First a set of Skyrme density functionals are obtained by optimizing the properties of finite nuclei and infinite nuclear matter around $n_{\rm sat}$. In particular, the neutron skin thickness of ^{208}Pb and ^{48}Ca are included. For finite nuclei, the binding energies and charge radii of 50 nuclei in the nuclear landscape are adopted, as described in [31]. To better describe finite nuclei and neutron stars simultaneously, a higher-order density-dependent term is added [31]. The fitting procedure is realized using the simulated annealing method. There is a competition in the fitting between properties of finite nuclei and the thick neutron skin. Hence the weights of the neutron skin thickness are varied to obtain different parameter sets. The EoS of nuclear matter is constructed based on obtained density functionals as well as the $npe\mu$ β equilibrium.

Next EoS at densities higher than $1.2n_{\rm sat}$ is constructed from the speed of sound without any details of nuclear interactions, according to Ref. [15]. The number density n can be obtained by the integral of sound speed in terms of the chemical potential μ from a starting density n_1, as $n(\mu) = n_1 \exp(\int_{\mu_1}^{\mu} \frac{d\mu'}{\mu' c_s^2})$. Then the pressure $p(\mu)$ is obtained by an additional integration of the number density $n(\mu)$ as $p(\mu) = p_1 + \int_{\mu_1}^{\mu} d\mu' n(\mu)$. Note that μ_1, p_1 correspond to values at the starting density n_1 to match EoSs given by density functionals. Since the sound speed is essentially unknown at intermediate densities, we adopt analytical curves to connect the starting n_1 and the peak location of c_s^2. In the first part from n_1 to the peak, we choose a monotonically increasing fourth-order polynomial curve after extensive tests. The details of the matching polynomial of c_s^2 are explained in the Appendixes. The polynomial coefficients are determined by two endpoints, in which both n_1 and the peak are varying. In the second part, the speed of sound is likely to decrease and finally matches $1/\sqrt{3}$. The second part only slightly affects massive neutron star observations. The possible zero c_s^2 related to the first-order phase transition is also allowed in the second part. The peak locations of c_s^2 are focused and heavily searched in this work, and the total computational costs are much less than the piecewise linear interpolation search in Refs. [15,16].

The astronomical observations of neutron stars are calculated by solving the well-known Tolman-Oppenheimer-Volkoff (TOV) equations. Based on EoS from density functionals and the speed of sound together, TOV equations are solved with varying initial densities at the neutron star center to obtain the mass-radius relationship. The tidal deformability Λ as a function of the neutron star mass can also be calculated by solving the TOV equation, as described in our previous work [32].

III. RESULTS

To implement constraints from the neutron skin of ^{208}Pb, we obtain three optimized Skyrme density functionals with different fitting weights, which correspond to $R_{\rm skin}^{208} = 0.22$, 0.247, 0.284 fm, respectively. The details of the three new

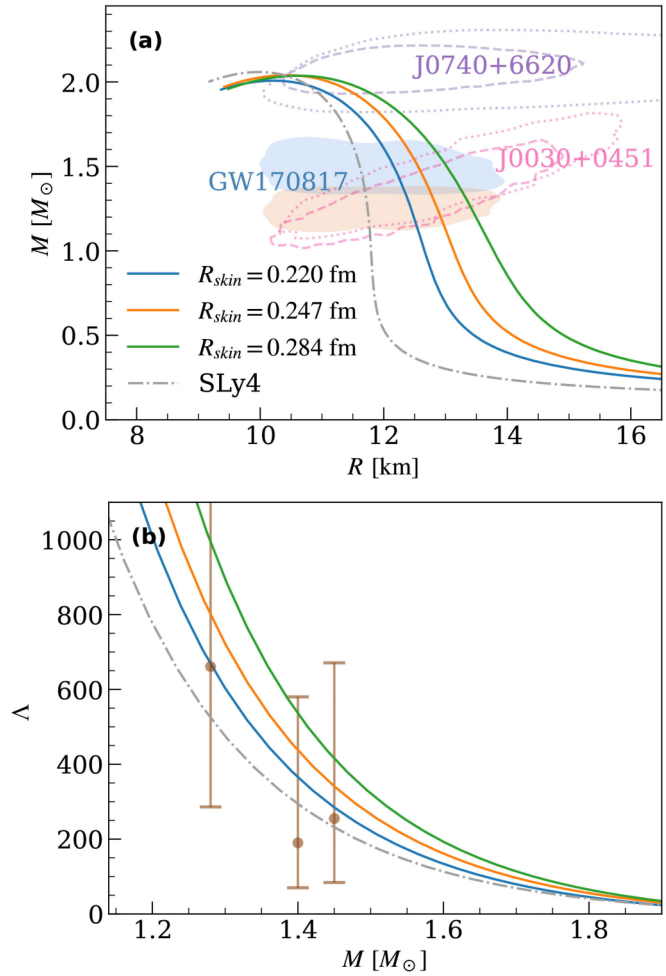

FIG. 1. Calculated neutron star observations with different density functionals associated with varying neutron skin thickness of ^{208}Pb. (a) The mass-radius curves; (b) the calculated tidal deformability Λ and the GW170817 inferences [2].

Skyrme interactions are given in the Appendixes. The resulting mass-radius relations of neutron stars are shown in Fig. 1. Note that EoS employed in Fig. 1 are based on Skyrme interactions in the full density range, without any modifications of speed of sound. For comparison, results of SLy4 [17] are also shown, which corresponds to $R_{\rm skin}^{208} = 0.16$ fm. We can see that, with an increasing $R_{\rm skin}^{208}$, the radius and tidal deformability of a $1.4M_\odot$ neutron star also increase, while the maximum masses all are around $2.0M_\odot$. For results corresponding to $R_{\rm skin}^{208} = 0.284$ fm, which is close to the PREX-II experiment, the associated radius and tidal deformability of a $1.4M_\odot$ neutron star are in tension with the GW170817 observations, in which $\Lambda = 190^{+390}_{-120}$ [2]. Such tension is more serious in the relativistic mean-field framework [13]. All density functionals cannot reproduce the massive neutron star in PSR $J0740+6620$ from NICER and XMM-Newton observations [33,34].

To reconcile the thick neutron skin with astronomical observations of neutron stars, the varying speed of sound is constructed starting from $n_1 = 1.2$, 1.5, $1.8\,n_{\rm sat}$. After heavy searches, we find that an early softening speed of sound is

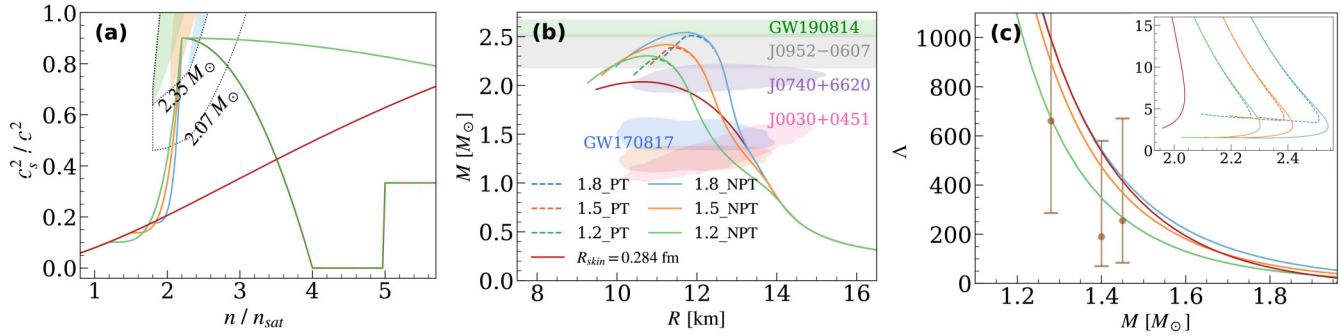

FIG. 2. Neutron star observations based on EoS from the combination of the density functional of the thick neutron skin and different speed of sound. (a) Exotic structures of speed of sound with constrained peak regions, in which constraints of maximum masses above 2.35 and 2.07 $M_\odot$ are shown; (b) the mass-radius curves corresponding to different c_s^2 in (a), in which structures with (PT) and without (NPT) the first-order phase transition are compared; (c) the tidal deformability Λ associated with different speed of sound in (a).

required to reduce the radius and tidal deformability of a $1.4M_\odot$ neutron star. Then a steep-rising speed of sound is required to obtain the reported maximum mass. With earlier modifications of the speed of sound, there are larger rooms to adjust c_s to reproduce astronomical observations. Similarly, the starting density n_1 is adopted as $1.1n_{\rm sat}$ in Refs. [15,16]. Calculations show that neutron star observations are sensitive to the speed of sound below $3n_{\rm sat}$ and are barely dependent on details of c_s^2 at higher densities. It can seen that, by employing exotic structures in speed of sound, the observations of neutron stars in GW170817 [2], $J0030+0451$ [3,4], $J0740+6620$ [33,34] can now be described simultaneously. The slightly softening sound speed at the beginning is crucial to satisfy the tidal deformability of neutron stars in GW170817. In Ref. [12], the statistical analysis also finds that a softening of speed of sound is possible when the slope of symmetry energy is larger than 100 MeV. Moreover, the reported heaviest neutron star of $2.35M_\odot$ in pulsar J0952-0607 [35] would inevitably invoke a steep-rising speed of sound. In Fig. 2(b), a possible neutron star of $2.6M_\odot$ in the GW190814 event [36] can be reached with $n_1 = 1.8n_{\rm sat}$, but it violates the tidal deformability constraints. The peak in Fig. 2(a) is at $2.2n_{\rm sat}$, and by shifting the peak to $1.9n_{\rm sat}$, a $2.6M_\odot$ neutron star can also be reached with $n_1 = 1.2n_{\rm sat}$. However, it is difficult to reach $2.6M_\odot$ by applying the tidal deformability constraint at $1.4M_\odot$ with the thick $R_{\rm skin}^{208}$, as shown in Fig. 3. Note that whether it is a massive neutron star or a light black hole is still in disputation [37].

One crucial question is to search for the allowed region of peak locations in speed of sound. For the thick $R_{\rm skin}^{208}$, the exotic structures in sound speed are inevitable even for a $2.0M_\odot$ neutron star based on heavy searches. In Fig. 2(a), the allowed region of the peak locations with constraints on maximum masses at $2.07M_\odot$ [33,34] and $2.35M_\odot$ [35] are shown. The left boundaries are determined by the tidal deformability $\Lambda = 519$ at $1.4M_\odot$, as suggested by a comprehensive study [38], which is a slightly more stringent constraint compared to the observational upper limit at 580 [2]. It can be seen that with combined constraints of $2.35M_\odot$, $\Lambda = 519$, and the thick $R_{\rm skin}^{208}$, the allowed region of the peak locations is rather shrunk. With different n_1, the corresponding allowed peak area is rather small, as indicated by different shadow colors in Fig. 2(a). The searches show that $n_1 = 1.8n_{\rm sat}$ is too late to describe GW170817 observations.

The possible first-order phase transitions with zero speed of sound at $4n_{\rm sat}$ are also displayed in Fig. 2. The observations of such sharp phase transitions are different from those of smooth transitions only in neutron stars around the maximum masses. We see that there are possible two neutron stars with similar masses but different radii, called twins, as an evidence of phase transition. However, their difference in the tidal deformability is small and only exhibits in massive neutron stars, as shown in Fig. 2(c).

The sharp first-order phase transition from nuclear matter to exotic quark matter is believed to exist, e.g., as predicted to be around $\mu \approx 1200$ MeV in the QCD phase diagram [39], but it is a tremendous challenge to determine the actual transition point. To explore the possible scenario of phase transition, the consequences of different transition points from 3.0 to 4.5 $n_{\rm sat}$

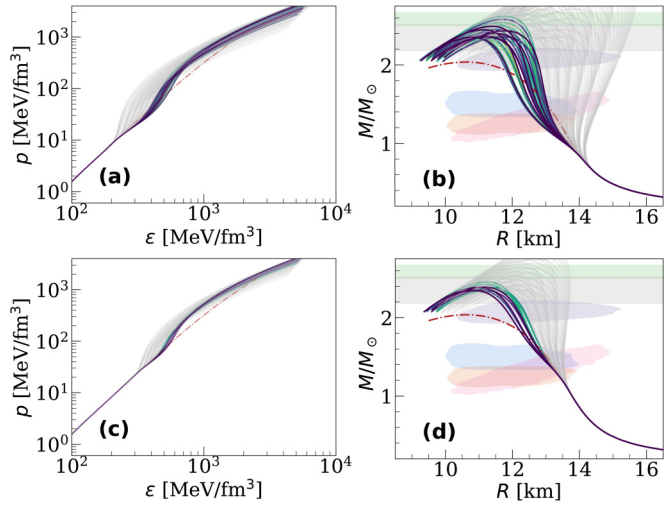

FIG. 3. EoS and neutron star observations by searching the speed of sound associated with the thick $R_{\rm skin}^{208}$, in which the results beyond $\Lambda = 519$ at $1.4M_\odot$ are shown in gray color. (a) The search of EoS with the starting density $n_1 = 1.2n_{\rm sat}$; (b) the resulting mass-radius curves with $n_1 = 1.2n_{\rm sat}$; (c) EoS with $n_1 = 1.8n_{\rm sat}$; (d) mass-radius curves with $n_1 = 1.8n_{\rm sat}$.

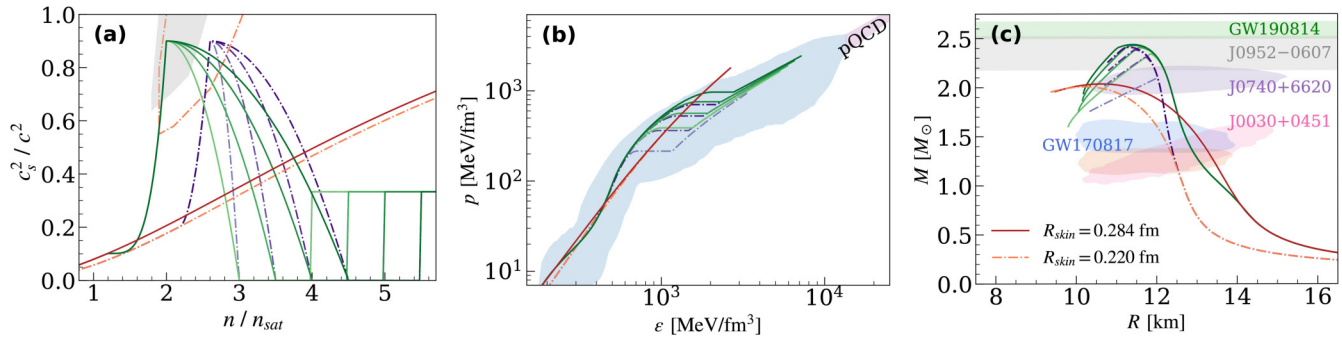

FIG. 4. EoS and neutron star observations associated with different first-order phase transitions. (a) The speed of sound with different first-order phase transitions, and the allowed peak regions associated with thick (shadow) and thin (orange dashed contour) neutron skins are displayed. (b) The pressure corresponding to different sound speed in (a) and the allowed boundaries taken from Ref. [15]; (c) the mass-radius curves obtained with EoS in (b).

are compared in Fig. 4. The energy densities ϵ (or in chemical potential μ) at 3.0, 3.5, 4.0, and 4.5 $n_{\rm sat}$ are 920.2, 1215.9, 1547.2, 1913.2 MeV fm^{-3}, respectively. In Fig. 4, the starting density n_1 is fixed as $1.2n_{\rm sat}$, and the peak location of c_s^2 is at $2.0n_{\rm sat}$. For the thinner $R_{\rm skin}^{208}$ of 0.22 fm, the allowed region of peak locations is much extended. The phase transitions with the thinner $R_{\rm skin}^{208}$ are also shown for comparison, in which the peak is at $2.6n_{\rm sat}$.

The EoS associated with different speed of sound in Fig. 4(a) and the resulting mass-radius curves are shown in Figs. 4(b) and 4(c), respectively. For the thick neutron skin, the slight dip in c_s^2 following $1.2n_{\rm sat}$ causes a small softening deviation from the original EoS. Such a small deviation of EoS is indispensable for describing neutron stars of $1.4M_\odot$. For the steep-rising or rapid-decreasing structures in the speed of sound, the corresponding EoS changes rather moderately. Finally the EoS approaches the conformal limit of $c_s^2 = 1/3$. The allowed region of EoS from large-scale searches [15] is also shown. For the thick neutron skin, EoS related to the phase transition at densities $\geqslant 4.5n_{\rm sat}$ is reaching the allowed boundaries. In addition, an early peak location with a delayed transition point is not consistent with a rapid drop of c_s^2 in a first-order phase transition [18,40]. This indicates that an early first-order phase transition is more favorable with thick neutron skins. For the thin neutron skin, the allowed peak region is larger and extends to higher densities. Actually the combination of a delayed peak location and an early transition point is problematic. For the transition point at $3.0n_{\rm sat}$ and the peak at $2.6n_{\rm sat}$, the maximum mass of $2.35M_\odot$ cannot be reached, as shown in Fig. 4(c). This implies that a considerable coexisting region of hadrons and quarks before the first-order phase transition is needed to support $2.35M_\odot$ for both thin and thick neutron skins. For the thin neutron skin, there is less preference in the transition point due to the extended peak area. The higher peak region associated with the thick neutron skin also means that the phase transition is stronger. Hence an early and strong first-order phase transition is comparatively more favorable for the thick neutron skin due to the stringent peak region. Note that an early first-order phase transition indicates the existence of large quark cores in neutron stars.

IV. DISCUSSIONS

The present study is based on the astonishing thick neutron skin of ^{208}Pb in experiments. Note that there are large uncertainties in measurements [10]. The simultaneous description of several nuclear observables and neutron skin measurements is very challenging [41]. The first-principle calculations of nuclear matter above saturation density are extremely difficult and uncertainties grow rapidly [7,42]. *Ab initio* nuclear calculations are actually based on renormalized two- and three-body interactions in reduced configuration spaces [7,11,42], and omitted contributions of many-body short-range hard-core interactions could explosively increase at high densities. In fact, the average distance between nucleons is 1.46 fm at $2.0n_{\rm sat}$ in the cubic packing and nucleons are already strongly overlapped considering that the nucleon radius is about 0.8 fm. The threshold distance of 1.6 fm corresponds to $1.5n_{\rm sat}$. This means current theoretical framework is questionable at $2.0n_{\rm sat}$ and the steep-rising structure in sound speed cannot be excluded. After the starting density n_1, EoS is required to soften slightly and this could be due to the appearance of hyperons [43]. The softening EoS after the peak can be understood as the influences of deconfined quarks. Very recently a possible light neutron star is observed with a mass of $0.77M_\odot$ and a radius of 10.4 km [44]. If this object is a neutron star, then very early softening of speed of sound is required and this is not favorable for a thick neutron skin. Therefore a more precise measurement of neutron skin is highly expected because it has significant consequences.

V. CONCLUSION

The surprising thick neutron skin of ^{208}Pb is taken into account to constrain the speed of sound in neutron stars. As a result, exotic structures in speed of sound are required, consisting of a small softening slope at the starting density 1.2–1.5 $n_{\rm sat}$ followed by a steep rising peak around $2.0n_{\rm sat}$. This exotic structures can successfully describe existing massive neutron stars and gravitational wave observations simultaneously. Due to the stringent allowed region of peak locations in the case of thick neutron skins, an early and

strong first-order phase transition is more favorable. For the thin neutron skin, the allowed peak region is much extended and thus has less preference in the transition point. We reveal that the thick neutron skin has significant implications in the speed of sound at intermediate densities, the appearance of hyperons and the first-order phase transitions, thus more precise measurements of $R_{\rm skin}^{208}$ are highly expected.

ACKNOWLEDGMENTS

We are grateful for discussions with L. W. Chen and F. R. Xu. This work was supported by the National Key R&D Program of China (Grant No. 2023YFE0101500) and National Natural Science Foundation of China under Grants No. 11975032, No. 11835001, No. 12335007, and No. 11961141003. We also acknowledge the funding support from the State Key Laboratory of Nuclear Physics and Technology, Peking University (No. NPT2023ZX01).

APPENDIX A: MATCHING POLYNOMIAL OF SPEED OF SOUND

For the thick neutron skin, the square of speed of sound c_s^2 to connect the starting point and the peak location is constructed as

$$y = y_1 + (y_2 - y_1)\cdot\left(\frac{x - x_1}{x_2 - x_1}\right)^4,$$

where c_s^2 as a function of density x is written as y, the starting point of c_s^2 is y_1 and the end point is y_2. The starting density is x_1 and the end density is x_2. The end point (x_2, y_2) is called the peak location of c_s^2.

For the thin neutron skin, c_s^2 to connect the starting point $(x_1,\ y_1)$ and the peak location $(x_2,\ y_2)$ is constructed as a second-order polynomial

$$y = y_1 + \frac{y_2 - y_1}{\Delta y_0}\cdot\left[\left((x - x_1)\cdot\frac{\Delta x_0}{x_2 - x_1} + x_{01}\right)^2 - y_{01}\right],$$

$$x_{01} = 0.1,\ x_{02} = 1.1,\ y_{01} = x_{01}^2,$$

$$\Delta x_0 = x_{01} - x_{02} = 1,$$

$$\Delta y_0 = x_{01}^2 - x_{02}^2.$$

After the peak locations, c_s^2 decreases rapidly from the peak to zero at density x_3. This is a coexisting region before the first-order phase transition, where c_s^2 is constructed as

$$y = y_2 + \frac{y_3 - y_2}{\Delta y_0}\cdot\left((x - x_2)\cdot\frac{\Delta x_0}{x_3 - x_2}\right)^2,$$

$$\Delta x_0 = 1,$$

$$\Delta y_0 = (\Delta x_0)^2,$$

$$y_3 = 0.$$

The first-order phase transition is in the range with zero speed of sound, in which the pressure is not changed with increasing densities.

For higher-order phase transitions, c_s^2 decreases smoothly from the peak to the conformal limit of $1/3$, and is constructed as

$$y = y_2 + \frac{y_3 - y_2}{\Delta y_0}\cdot(1 - e^{-((x-x_2)\cdot\frac{\Delta x_0}{x_3 - x_2})^2}),$$

$$\Delta x_0 = 5,$$

$$\Delta y_0 = 1 - e^{-(\Delta x_0)^2},$$

$$y_3 = 1/3,$$

$$x_3 = 40.0.$$

APPENDIX B: NEW EXTENDED SKYRME INTERACTIONS

The Skyrme interaction is a sum of two-body interaction and three-body interaction:

$$V_{\rm Skyrme} = \sum_{i<j} v_{ij}^{(2)} + \sum_{i<j<k} v_{ijk}^{(3)},$$

$$\begin{aligned} v_{ij}^{(2)} &= t_0(1 + x_0P_\sigma)\delta(\boldsymbol{r}_i - \boldsymbol{r}_j) \\ &\quad + \frac{1}{2}t_1(1 + x_1P_\sigma)[\delta(\boldsymbol{r}_i - \boldsymbol{r}_j)\mathbf{k}^2 + \mathbf{k}'^2\delta(\boldsymbol{r}_i - \boldsymbol{r}_j)] \\ &\quad + t_2(1 + x_2P_\sigma)\mathbf{k}'\cdot\delta(\boldsymbol{r}_i - \boldsymbol{r}_j)\mathbf{k} \\ &\quad + iW_0(\sigma_i + \sigma_j)\cdot\mathbf{k}'\times\delta(\boldsymbol{r}_i - \boldsymbol{r}_j)\mathbf{k}. \end{aligned}$$

The standard spin-orbit Hamiltonian involves one parameter W_0 and has been extended to include isospin dependence [45] as

$$H_{so} = -b_4\left(\rho\nabla\cdot\mathbf{J} + b_4'\sum_q \rho_q\nabla\cdot\mathbf{J}_q\right).$$

TABLE I. The fitted Skyrme parameters in this work are listed. The symmetry energy J, the density slope L of the symmetry energy, the incompressibility coefficient K_∞ at the saturation density are given.

Parameters	Set I	Set II	Set III
t_0	−2340.20	−2287.31	−2339.41
t_1	455.64	475.35	472.89
t_2	−399.65	−465.37	−462.58
t_3	11564.79	10955.19	11709.66
t_{3E}	2887.07	3217.65	2620.65
x_0	2.41×10^{-2}	−0.303	−0.649
x_1	−0.309	−0.243	−0.243
x_2	−0.718	−0.763	−0.763
x_3	−0.193	−0.874	−1.414
x_{3E}	1.100	1.586	1.935
b_4	68.16	97.38	96.11
b_4'	98.69	74.60	79.35
γ	1/6	1/6	1/6
γ_E	0.5	0.5	0.5
J (MeV)	35.614	34.624	38.062
L (MeV)	46.653	60.077	81.659
e_∞ (MeV)	−16.03	−16.01	−15.98
K_∞ (MeV)	239.00	238.64	233.39
$R_{\rm skin}^{208}$ (fm)	0.220	0.247	0.284

The three-body interaction is written as a density dependent two-body interaction, in which an additional higher-order density dependent term is added [31]:

$$v_{ijk}^{(3)} = \tfrac{1}{6}t_3(1 + x_3P_\sigma)\rho(\boldsymbol{R})^\gamma\delta(\boldsymbol{r}_i - \boldsymbol{r}_j) + \tfrac{1}{6}t_{3E}(1 + x_{3E}P_\sigma)\rho(\boldsymbol{R})^{\gamma_E}\delta(\boldsymbol{r}_i - \boldsymbol{r}_j).$$

t_i, x_i, b_4, and b'_4 are parameters of the Skyrme interaction. Also, t_{3E} and x_{3E} are additional high-order parameters. Three sets of parameters are fitted by including the neutron skin measurements with different weights, as listed in Table I.

[1] B. P. Abbott, R. Abbott, T. D. Abbott, F. Acernese, K. Ackley, C. Adams, T. Adams, P. Addesso, R. X. Adhikari, V. B. Adya *et al.* (LIGO Scientific Collaboration and Virgo Collaboration), Phys. Rev. Lett. **119**, 161101 (2017).

[2] B. P. Abbott, R. Abbott, T. D. Abbott, F. Acernese, K. Ackley, C. Adams, T. Adams, P. Addesso, R. X. Adhikari, V. B. Adya *et al.* (The LIGO Scientific Collaboration and the Virgo Collaboration), Phys. Rev. Lett. **121**, 161101 (2018).

[3] M. C. Miller, F. K. Lamb, A. J. Dittmann, S. Bogdanov, Z. Arzoumanian, K. C. Gendreau, S. Guillot, A. K. Harding, W. C. G. Ho, J. M. Lattimer *et al.*, Astrophys. J. Lett. **887**, L24 (2019).

[4] T. E. Riley, A. L. Watts, S. Bogdanov, P. S. Ray, R. M. Ludlam, S. Guillot, Z. Arzoumanian, C. L. Baker, A. V. Bilous, D. Chakrabarty *et al.*, Astrophys. J. Lett. **887**, L21 (2019).

[5] A. Sorensen, K. Agarwal, K. W. Brown, Z. Chajęcki, P. Danielewicz, C. Drischler, S. Gandolfi, J. W. Holt, M. Kaminski, C.-M. Ko *et al.*, Prog. Part. Nucl. Phys. **134**, 104080 (2024).

[6] P. Li, J. Steinheimer, T. Reichert, A. Kittiratpattana, M. Bleicher, and Q. Li, Sci. China-Phys. Mech. Astron. **66**, 232011 (2023).

[7] I. Tews, J. Carlson, S. Gandolfi, and S. Reddy, Astrophys. J. **860**, 149 (2018).

[8] O. Komoltsev and A. Kurkela, Phys. Rev. Lett. **128**, 202701 (2022).

[9] S. Abrahamyan, Z. Ahmed, H. Albataineh, K. Aniol, D. S. Armstrong, W. Armstrong, T. Averett, B. Babineau, A. Barbieri, V. Bellini, R. Beminiwattha, J. Benesch, F. Benmokhtar, T. Bielarski, W. Boeglin, A. Camsonne, M. Canan, P. Carter, G. D. Cates, C. Chen *et al.* (PREX Collaboration), Phys. Rev. Lett. **108**, 112502 (2012).

[10] D. Adhikari, H. Albataineh, D. Androic, K. Aniol, D. S. Armstrong, T. Averett, C. Ayerbe Gayoso, S. Barcus, V. Bellini, R. S. Beminiwattha *et al.* (PREX Collaboration), Phys. Rev. Lett. **126**, 172502 (2021).

[11] B. Hu, W. Jiang, T. Miyagi, Z. Sun, A. Ekström, C. Forssén, G. Hagen, J. D. Holt, T. Papenbrock, S. R. Stroberg, and I. Vernon, Nat. Phys. **18**, 1196 (2022).

[12] R. Essick, I. Tews, P. Landry, and A. Schwenk, Phys. Rev. Lett. **127**, 192701 (2021).

[13] B. T. Reed, F. J. Fattoyev, C. J. Horowitz, and J. Piekarewicz, Phys. Rev. Lett. **126**, 172503 (2021).

[14] D. Adhikari, H. Albataineh, D. Androic, K. A. Aniol, D. S. Armstrong, T. Averett, C. Ayerbe Gayoso, S. K. Barcus, V. Bellini, R. S. Beminiwattha *et al.*, Phys. Rev. Lett. **129**, 042501 (2022).

[15] E. Annala, T. Gorda, A. Kurkela, J. Nättilä, and A. Vuorinen, Nat. Phys. **16**, 907 (2020).

[16] S. Altiparmak, C. Ecker, and L. Rezzolla, Astrophys. J. Lett. **939**, L34 (2022).

[17] E. Chabanat, P. Bonche, P. Haensel, J. Meyer, and R. Schaeffer, Nucl. Phys. A **635**, 231 (1998).

[18] H. Tan, T. Dore, V. Dexheimer, J. Noronha-Hostler, and N. Yunes, Phys. Rev. D **105**, 023018 (2022).

[19] E. Annala, T. Gorda, E. Katerini, A. Kurkela, J. Nättilä, V. Paschalidis, and A. Vuorinen, Phys. Rev. X **12**, 011058 (2022).

[20] P.-G. Reinhard, X. Roca-Maza, and W. Nazarewicz, Phys. Rev. Lett. **127**, 232501 (2021).

[21] J. J. Li, A. Sedrakian, and M. Alford, Astrophys. J. **944**, 206 (2023).

[22] W. G. Newton, R. Preston, L. Balliet, and M. Ross, Phys. Lett. B **834**, 137481 (2022).

[23] W. J. Xie, Z. W. Ma, and J. H. Guo, Nucl. Sci. Tech. **34**, 91 (2023).

[24] Z. Zhang and L. W. Chen, Phys. Rev. C **108**, 024317 (2023).

[25] A. Kanakis-Pegios, P. S. Koliogiannis, and Ch. C. Moustakidis, Phys. Rev. C **102**, 055801 (2020).

[26] G. Grams, R. Somasundaram, J. Margueron, and E. Khan, Phys. Rev. C **106**, 044305 (2022).

[27] C. Drischler, S. Han, and S. Reddy, Phys. Rev. C **105**, 035808 (2022).

[28] B. Reed and C. J. Horowitz, Phys. Rev. C **101**, 045803 (2020).

[29] R. Somasundaram, I. Tews, and J. Margueron, Phys. Rev. C **107**, 025801 (2023).

[30] Z. Bai and Y. X. Liu, Phys. Rev. D **108**, 014018 (2023).

[31] X. Y. Xiong, J. C. Pei, and W. J. Chen, Phys. Rev. C **93**, 024311 (2016).

[32] C. J. Jiang, Y. Qiang, D. W. Guan, Q. Z. Chai, C. Y. Qiao, and J. C. Pei, Chin. Phys. Lett. **38**, 052101 (2021).

[33] M. C. Miller, F. K. Lamb, A. J. Dittmann, S. Bogdanov, Z. Arzoumanian, K. C. Gendreau, S. Guillot, W. C. G. Ho, J. M. Lattimer, M. Loewenstein *et al.*, Astrophys. J. Lett. **918**, L28 (2021).

[34] T. E. Riley, A. L. Watts, P. S. Ray, S. Bogdanov, S. Guillot, S. M. Morsink, A. V. Bilous, Z. Arzoumanian, D. Choudhury, J. S. Deneva *et al.*, Astrophys. J. Lett. **918**, L27 (2021).

[35] R. W. Romani, D. Kandel, A. V. Filippenko, T. G. Brink, and W. K. Zheng, Astrophys. J. Lett. **934**, L17 (2022).

[36] R. Abbott, T. D. Abbott, S. Abraham, F. Acernese, K. Ackley, C. Adams, R. X. Adhikari, V. B. Adya, C. Affeldt, M. Agatho *et al.*, Astrophys. J. Lett. **896**, L44 (2020).

[37] F. J. Fattoyev, C. J. Horowitz, J. Piekarewicz, and B. Reed, Phys. Rev. C **102**, 065805 (2020).

[38] Y. Lim and J. W. Holt, Phys. Rev. Lett. **121**, 062701 (2018).

[39] Reaching for the Horizon: The 2015 Long Range Plan for Nuclear Science, https://www.osti.gov/biblio/1296778-reaching-horizon-long-range-plan-nuclear-science, 2015.

[40] S. Benić, D. Blaschke, D. E. Alvarez-Castillo, T. Fischer, and S. Typel, Astron. Astrophys. **577**, A40 (2015).

[41] P.-G. Reinhard, X. Roca-Maza, and W. Nazarewicz, Phys. Rev. Lett. **129**, 232501 (2022).
[42] C. Drischler, R. J. Furnstahl, J. A. Melendez, and D. R. Phillips, Phys. Rev. Lett. **125**, 202702 (2020).
[43] J. M. Lattimer and M. Prakash, Phys. Rep. **442**, 109 (2007).
[44] V. Doroshenko, V. Suleimanov, G. Pühlhofer, and A. Santangelo, Nat. Astron. **6**, 1444 (2022).
[45] P.-G. Reinhard and H. Flocard, Nucl. Phys. A **584**, 467 (1995).